JOURNAL OF AIRCRAFT
Vol. 47, No. 2, March–April 2010

Aeroelastic Behavior of Flat Plates Moving Near the Ground

Abdullah O. Nuhait*
King Saud University, Riyadh 11421, Saudi Arabia
and
Dean T. Mook†
Virginia Polytechnic Institute and State University, Blacksburg, Virginia 24061

DOI: 10.2514/1.41186

An aeroelastic model based on a two-dimensional unsteady vortex-lattice method is used to study the dynamic behavior of elastically supported flat plates interacting with an incompressible uniform flow near the ground. The ground effect is simulated by the image technique. The air and the plate together are treated as a single dynamic system, and all of the equations of motion are integrated simultaneously and interactively in the time domain by means of an iterative scheme based on predictor–corrector techniques. The present results show that the plates are destabilized by the proximity to the ground: the lower the height, the lower the airspeed at the onset of flutter. No structural damping was included in the present model, but damping is expected to raise the critical airspeed. The complete aeroelastic model is general and versatile; the aerodynamic model is inherently nonlinear and the structural model may be either linear or nonlinear. As the amplitude of the flutter motion grows, the nonlinear aerodynamic model caps the motion, which results in a limit cycle. Moreover, the extension to three dimensions is straightforward.

Nomenclature

a = location of the elastic axis e relative to the midchord of the plate n in terms of $c/2$
a_h = amplitude of plunging motion
a_θ = amplitude of pitching motion
$\mathbf{b}_2$ = unit vector in the y direction
c = plate chord
C = Theodorsen's function used in Eqs. (5) and (6)
CG = center of mass
C_l = lift coefficient
C_m = pitching-moment coefficient
C_n = normal-force coefficient
C_p = pressure coefficient
e = location of the elastic axis
H = nominal height of the elastic axis above ground divided by c
$h(t)$ = vertical translational degree of freedom
$\dot{h}$ = plunging velocity
$\bar{h}$ = amplitude of plunging oscillation in Eqs. (5) and (6)
I_e = mass moment of inertia about the elastic axis
$\mathbf{j}$ = unit vector in the Y direction
K_h = translational spring stiffness
K_θ = torsional spring stiffness
K_0 = Bessel's function of zero order
K_1 = Bessel's function of first order
k = reduced frequency in Eqs. (5) and (6), $(c/2)(\omega_f/V_c)$
l = length of the bound element
l_h = coefficient used in Eqs. (5) and (6)
l_θ = coefficient used in Eqs. (5) and (6)
M = aerodynamic moment
m = mass of plate per unit span
m_h = coefficient used in Eqs. (5) and (6)
m_θ = coefficient used in Eqs. (5) and (6)
N = aerodynamic force
N_{el} = number of bound elements
$\mathbf{n}$ = unit normal vector
p = pressure
$\mathbf{r}$ = position vector
r = dimensionless radius of gyration about the elastic axis, $r^2 = (4/c^2)(I_e/m)$
t = time
U = speed characterizing motion of the plate
V = reduced airspeed, $(2/c)(U/\omega_\theta)$
$\mathbf{V}$ = velocity vector
V_c = critical airspeed computed by Eq. (12)
V_e = linear velocity of the origin of the body-fixed frame
V_m = velocity induced by all discrete vortices of the plate, its wake, and their images
XYZ = ground-fixed coordinates
xyz = body-fixed coordinates
x_0 = location of the center of mass CG relative to the elastic axis in terms of $c/2$
Γ_{c_1} = circulation of the starting vortex
Γ_j = circulation of the bound vortices
ΔC_p = pressure-jump coefficient across the plate, $(2/\rho_\infty)(\Delta P/U^2)$
Δp = pressure jump across the plate
Δt = time step
θ = angle of rotation
$\dot{\theta}$ = angular velocity about the elastic axis
$\bar{\theta}$ = amplitude of pitching oscillation in Eqs. (5) and (6)
μ = mass ratio, $(1/\pi)(4/c^2)(m/\rho_\infty)$
ρ_∞ = density of air
σ = plunging-pitching frequency ratio, ω_h/ω_θ
ϕ = velocity potential
ω_f = flutter frequency in Eqs. (5) and (6)
ω_h = uncoupled natural plunging frequency of the plate
ω_θ = uncoupled natural pitching frequency of the plate about the elastic axis

Received 30 September 2008; revision received 9 October 2009; accepted for publication 2 December 2009.

*Associate Professor, Mechanical Engineering Department; anuhait@hotmail.com.
†N. Waldo Harrison Professor Emeritus, Engineering Science and Mechanics Department; dmook@vt.edu. Associate Fellow AIAA.

I. Introduction

THE ongoing development of uninhabited air vehicles (UAVs) intended for high-altitude, long-endurance (HALE) missions has introduced new considerations, challenges, and opportunities. To enhance their efficiency, one is immediately led to consider very-high-aspect-ratio wings. Increasing the aspect ratio and, consequently, the flexibility makes the wing more vulnerable to aeroelastic instability.

Moreover, the analysis of such wings is more complicated because of the necessity of using nonlinear aerodynamic and, possibly, structural models. As various strategies to enhance the performance of HALE UAVs emerge, it may be that some aircraft will operate outside the nominal flutter envelope by using active controls to suppress the aeroelastic instability and gust response in a way similar to how the flight dynamics of modern fighters are stabilized. Such an innovative design could significantly reduce the weight of the airframe, both enhancing performance and reducing cost. For these aircraft, unlike conventional ones, dynamic aeroelastic stability during the ground roll and/or while ground effect is still strong may be an important consideration. In this paper, as a preliminary step, the behavior of an elastically supported rigid plate in a uniform stream near the ground is investigated.

The behavior of rigid plates in uniform streams covers a large and important part of the field of aeroelasticity. In 1935, Theodorsen [1] studied the dynamic stability of rigid wing sections having two or three degrees of freedom. A huge body of research based on his work was subsequently established. Theodorsen used the Kutta–Zhukovsky transformation to map a unit circle into a flat plate. The unit circle was represented with sources and sinks, and the Kutta condition was satisfied by introducing vortices in the wake and their images inside the circle. Later, Theodorsen and Garrick [2] studied the flutter of wing sections. Their model is a practical approximation to a large-aspect-ratio wing with a smooth slow variation in its spanwise characteristics. In addition, there are the texts by Scanlan and Rosenbaum [3], Fung [4], Bisplinghoff et al. [5], Bisplinghoff and Ashley [6], Hodges and Pierce [7], Dowell [8], and Païdoussis [9]. In spite of this wealth of research, the authors are not aware of any study of aeroelastic behavior of plates in ground effect, probably because such a study would not have addressed any practical need up to now, with the possible exception of wingships. Because ground effect can increase the lift above its value far from the ground, there has been some interest in designing wingships, which fly between 6 and 30 m above the sea (see, for example, Nuhait and Zedan [10]).

In the present aeroelastic model, the fluid and plate are treated as the elements of a single dynamic system, and the equations of motion for the plate, the flowfield, and the controller (if there is one) are integrated simultaneously and interactively in the time domain. The time-domain model describes transient aeroelastic behavior before, during, and after the onset of flutter, as long as the effective angles of attack are not large enough to produce stall. The aerodynamic loads are obtained from a 2-D unsteady vortex-lattice method developed by Nuhait and Zedan [11].

II. Aeroelastic Model

In Fig. 1 a rigid plate that is free to plunge and pitch is represented. The plate is modeled structurally as a uniformly distributed mass supported by translational and torsional springs (with constants K_h and K_θ, respectively) subjected to a transverse distributed loading $\Delta p(x,t)$, the pressure difference across the plate. Both springs are attached to the plate at the elastic axis e. The elastic axis is located at a distance $a(c/2)$ from the midchord, where c is the chord, and a is considered positive when the elastic axis is aft of the midchord. The center of mass CG is located at a distance $x_0(c/2)$ from the elastic axis; x_0 is positive when CG is aft of the elastic axis. In the system shown, the datum (at a fixed elevation) represents the fuselage of the aircraft; $h(t)$ and $\theta(t)$ represent the elastic deflections of the wing. The airspeed is considered to change slowly and is considered constant.

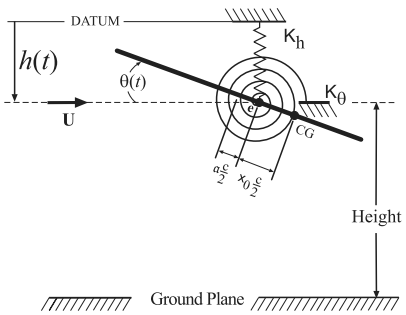

Fig. 1 A rigid plate supported by two linear springs with constants K_h and K_θ.

Two reference frames are used to describe the motion of the plate: XYZ is fixed to the ground (G-F), and xyz is fixed to the body (B-F), as shown in Fig. 2. Both frames are right-handed and the coordinate system XYZ is inertial, whereas the coordinate system xyz translates and rotates with the plate. The plate is allowed to translate (plunge) in the Z direction and to rotate (pitch) about the elastic axis in the X–Z plane. Plunging is denoted by h, and pitching is denoted by θ. The aerodynamic normal force is denoted by N, and the aerodynamic moment about the elastic axis is denoted by M.

The equations of motion are

$$m\left(\ddot{h}+x_0\frac{c}{2}\ddot{\theta}\cos\theta-x_0\frac{c}{2}\dot{\theta}^2\sin\theta\right)+K_h h=-\frac{1}{2}\rho_\infty U^2 c C_n\cos\theta \quad (1)$$

$$I_e\ddot{\theta}+mx_0\frac{c}{2}\ddot{h}\cos\theta+K_\theta\theta=\frac{1}{2}\rho_\infty U^2 c^2 C_m \quad (2)$$

where m is the mass of the plate, I_e is the mass moment of inertia about the elastic axis, C_n is the normal-force coefficient, and C_m is the pitching-moment coefficient about the elastic axis.

The two equations are nondimensionalized with the following characteristic parameters: U for speed, l for length, l/U for time, and ρ_∞ for air density. The resulting dimensionless equations of motion are

$$\ddot{h}=\left[\frac{1}{r^2-x_0^2\cos^2\theta}\right]\left[\frac{N_{\text{el}}}{2}x_0 r^2\sin\theta\dot{\theta}^2-\frac{4}{N_{\text{el}}^2}\frac{\sigma^2}{V^2}r^2 h+\frac{2}{N_{\text{el}}}\frac{1}{V^2}x_0 r^2\cos\theta\theta-\frac{2}{N_{\text{el}}}\frac{1}{\pi}\frac{1}{\mu}r^2 C_n\cos\theta-\frac{4}{N_{\text{el}}}\frac{1}{\pi}\frac{1}{\mu}x_0 C_m\cos\theta\right] \quad (3)$$

$$\ddot{\theta}=\left[\frac{1}{r^2-x_0^2\cos^2\theta}\right]\left[-x_0^2\cos\theta\sin\theta\dot{\theta}^2+\frac{8}{N_{\text{el}}^3}\frac{\sigma^2}{V^2}x_0\cos\theta h-\frac{4}{N_{\text{el}}^2}\frac{1}{V^2}r^2\theta+\frac{4}{Nel^2}\frac{1}{\pi}\frac{1}{\mu}x_0 C_n\cos^2\theta+\frac{8}{N_{\text{el}}^2}\frac{1}{\pi}\frac{1}{\mu}C_m\right] \quad (4)$$

where $\mu=(1/\pi)(4/c^2)(m/\rho_\infty)$ is the mass ratio; $r^2=(4/c^2)(I_e/m)$ is the dimensionless square of the radius of gyration about the elastic axis; $V=(2/c)(U/\omega_\theta)$ is the reduced airspeed; $\sigma=\omega_h/\omega_\theta$ is the frequency ratio in which $\omega_\theta^2=K_\theta/I_e$ and $\omega_h^2=K_h/m$ are the plate's natural pitching (about the elastic axis) and plunging frequencies, respectively; and N_{el} is the number of elements in the aerodynamic model. The characteristic length l has been replaced by c/N_{el}. Equations (1) and (2) are to be solved simultaneously for $h(t)$ and $\theta(t)$ explicitly.

The authors are not aware of experimental or numerical results for aeroelastic behavior in ground effect, so to provide confidence in

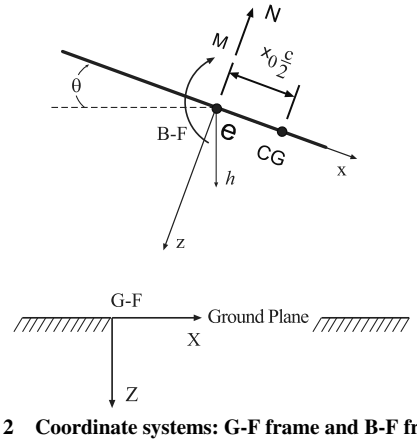

Fig. 2 Coordinate systems: G-F frame and B-F frame.

the present numerical model, we compare some results obtained with the present method with some results obtained with Theodorsen's method to predict the onset of flutter for a plate out of ground effect. In Theodorsen's method, the plunging and pitching motions are assumed to be harmonic, and the solution is obtained in the frequency domain. The linearized form of Eqs. (1) and (2), including Theodorsen's function, are

$$\left[\mu(1.0-\sigma^2\left(\frac{\omega_\theta}{\omega_f}\right)^2)+l_h\right]\bar{h}+\left[\mu x_0+l_\theta-l_h\left(\frac{1}{2}+a\right)\right]\bar{\theta}=0 \quad (5)$$

$$\left[\left(\mu x_0+m_h-l_h\left(\frac{1}{2}+a\right)\right)\right]\bar{h}+\left[\left(\mu r^2\left(1.0-\left(\frac{\omega_\theta}{\omega_f}\right)^2\right)\right.\right.$$
$$\left.\left.-\left(\frac{1}{2}+l_\theta\right)\left(\frac{1}{2}+a\right)+m_\theta+l_h\left(\frac{1}{2}+a\right)^2\right)\right]\bar{\theta}=0 \quad (6)$$

where ω_f is the flutter frequency, and $\bar{h}$ and $\bar{\theta}$ are the amplitudes of oscillations. The coefficient $m_h=\frac{1}{2}$, and the other coefficients l_h, l_θ, and m_θ are functions of reduced flutter frequency $k=(c/2)(\omega_f/V_c)$, where V_c is the critical (flutter) airspeed. Here, we used the following relations:

$$l_h=1-\frac{2iC}{k}, \qquad l_\theta=\frac{1}{2}-\frac{(1+2C)}{k}-2\frac{C}{k^2}, \qquad m_\theta=\frac{3}{8}-\frac{i}{k}$$

where C is Theodorsen's function and it is related to Bessel's functions K_0 and K_1:

$$C(k)=\frac{K_1(ki)}{K_1(ki)+K_0(ki)}$$

III. Aerodynamic Model

The flow is assumed to be 2-D, incompressible, and inviscid. As mentioned previously, two reference frames are used. All variables are written in dimensionless form using the same characteristic parameters introduced in the aeroelastic model. Dimensionless variables are

$$\mathbf{V}=\frac{\mathbf{V}^*}{U}, \qquad \phi=\frac{\phi^*}{Ul}, \qquad \mathbf{r}=\frac{\mathbf{r}^*}{l}, \qquad C_P=\frac{1}{2}\frac{p^*}{\rho_\infty U^2}$$

where $\mathbf{V}$, ϕ, $\mathbf{r}$, and C_P denote velocity, velocity potential, position vector, and pressure coefficient, respectively. The asterisk denotes the physical quantities.

The rigid plate, its wake, and their images are represented by sheets of vorticity, as shown in Fig. 3. The sheet representing the plate has its position specified and is called a *bound vortex sheet*; a pressure jump may exist across it. The sheet representing the wake, for which the position is not known in advance and is obtained as part of the solution, deforms freely and assumes a force-free position during the simulation. It is called a *free vortex sheet*. The bound and free vortex sheets are joined along the trailing edge of the plate.

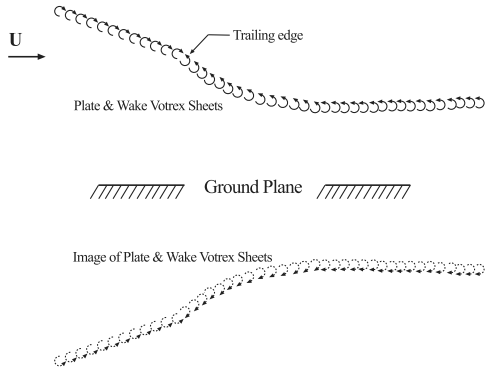

Fig. 3 Representation of the plate, its wake, and their images by continuous vortex sheets.

In the numerical model, the two vortex sheets are replaced with discrete vortices, as shown in Fig. 4. The total velocity field induced by these vortices must satisfy the continuity equation and the following six conditions:

1) $\mathbf{V}_{\text{disturbance}} \to 0$ far from the plate and its wake.

2) The no-penetration boundary condition is satisfied on the plate.

3) The vertical velocity component is zero on the ground plane.

4) The total circulation around a closed fluid line that encircles the plate and its wake is conserved (zero in this case).

5) The unsteady Kutta condition is satisfied at the trailing edge of the plate.

6) The pressure is continuous in the wake.

The plate is discretized into N_{el} equal-length panels (elements). Hence, the characteristic length l is equal to c/N_{el}. The vorticity distributed on each element is replaced by a single vortex of unknown strength Γ_j, located at one-fourth of the element length aft of its leading edge. The starting vortex is simulated by placing a vortex of unknown strength Γ_{c_1} at a point in the plane of the plate aft of the plate's trailing edge. As the number of elements increases, the location of the first-point vortex Γ_1 will approach the plate's leading edge, and the location of the starting vortex Γ_{c_1} will approach the plate's trailing edge.

The no-penetration boundary condition is imposed at one point (called a *control point*) on each element located at $3l/4$ aft of the leading edge of the element. The dimensionless length of the element is taken to be unity; hence, the dimensionless chord of the plate equals N_{el}.

The pressure jump Δp across each element is computed at the control point of that element by using the unsteady Bernoulli's equation. The pressure-jump coefficient ΔC_{p_i} at control point i is given by the following equation:

$$\Delta C_{p_i}=2\frac{\sum_{k=1}^{i}\Gamma_k(t+\Delta t)-\sum_{k=1}^{i}\Gamma_k(t)}{\Delta t}$$
$$+2\left(\frac{(\text{factor})\Gamma_i+\Gamma_{i+1}}{2}\mathbf{j}\times\mathbf{n}_i\right)\cdot(\mathbf{V}_m-[\mathbf{V}_e+\dot{\theta}\mathbf{b}_2\times\mathbf{r}])_i$$
$$\text{for } i=1,2,3,\ldots,N_{\text{el}} \quad (7)$$

where factor takes the value of 1, except for the first element, where it takes the value of 2; $\mathbf{V}_m$ is the velocity induced by all the discrete vortices of the plate, its wake, and their images at the control point; $\mathbf{V}_e$ is the linear velocity of the plate at point e, the origin of the B-F

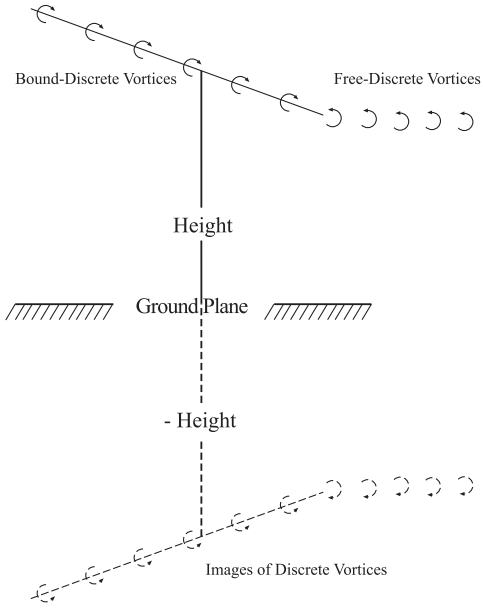

Fig. 4 Replacement of the continuous vortex sheets by discrete vortices.

frame, and the elastic axis, as shown in Fig. 2; and **r** is the position vector of the control point i with respect to point e. For more detail on the aerodynamic model, one is referred to the paper of Nuhait and Zedan [11]. The aerodynamic-load coefficients C_n and C_m are computed by integrating ΔC_{p_i} along the chord. The circulations around the discrete vortices that represent the wake are determined when these vortices are at the trailing edge and do not change as they are swept downstream. There is a flow around each vortex in the wake that affects the aerodynamic loads on the plate; hence, these loads depend on the history of the motion. The wake is the historian. As the discrete vortices move downstream, their influence on the plate decreases; hence, the historian has a fading memory.

IV. Method of Solution

The equations of motion (3) and (4), are rewritten as a set of first-order equations:

$$\dot{Y}_1 = Y_2 \tag{8}$$

$$\dot{Y}_2 = \left[\frac{1}{r^2 - x_0^2\cos^2 Y_3}\right]\left[\frac{N_{\text{el}}}{2}x_0 r^2 \sin Y_3 Y_4^2 - \frac{4}{N_{\text{el}}^2}\frac{\sigma^2}{V^2}r^2 Y_1 + \frac{2}{N_{\text{el}}}\frac{1}{V^2}x_0 r^2 \cos Y_3 Y_3 - \frac{2}{N_{\text{el}}}\frac{1}{\pi}\frac{1}{\mu}r^2 C_n \cos Y_3 - \frac{4}{N_{\text{el}}}\frac{1}{\pi}\frac{1}{\mu}x_0 C_m \cos Y_3\right] \tag{9}$$

$$\dot{Y}_3 = Y_4 \tag{10}$$

$$\dot{Y}_4 = \left[\frac{1}{r^2 - x_0^2\cos^2 Y_3}\right]\left[-x_0^2 \cos Y_3 \sin Y_3 Y_4^2 + \frac{8}{N_{\text{el}}^3}\frac{\sigma^2}{V^2}x_0 \cos Y_3 Y_1 - \frac{4}{N_{\text{el}}^2}\frac{1}{V^2}r^2 Y_3 + \frac{4}{N_{\text{el}}^2}\frac{1}{\pi}\frac{1}{\mu}x_0 C_n \cos^2 Y_3 + \frac{8}{N_{\text{el}}^2}\frac{1}{\pi}\frac{1}{\mu}C_m\right] \tag{11}$$

Aeroelastic behavior in incompressible flow depends on six dimensionless parameters characterizing the plate and airstream: x_0, a, σ, r^2, μ, and V. The first four of these describe the plate and its supporting mechanism. The mass ratio $\mu = (1/\pi)(4/c^2)(m/\rho_\infty)$ couples the plate to the flow through the relative densities. The dimensionless airspeed $V = (2/c)(U/\omega_\theta)$ is considered as the independent parameter. The equations of motion (8–11) are integrated numerically to find the plunging and pitching responses of the plate and the flow around the plate.

In this paper, the approach is to integrate all of the governing equations numerically, simultaneously, and interactively in the time domain. There is a fundamental complication with this approach: to predict the aerodynamic loads, one must know the motion of the plate, and to predict the motion of the plate, one must know the aerodynamic loads. To overcome this apparent impasse, an iterative scheme based on Hamming's fourth-order predictor–corrector method (Carnahan et al. [12]) is employed, and hence the added mass, the added damping, and/or added stiffness will not appear explicitly in the equations of motion.

Numerical experiments have shown that when the dimensionless time step Δt is set equal to unity, the aerodynamic model works best and the present numerical scheme uses integral time steps. Hamming's method requires the solution to be known at three previous time steps, which can be obtained by a variety of procedures.

V. Results and Discussions

A. Validation of Present Model

A plate similar to the one given in the report of Theodorsen and Garrick [2] is assumed; its properties are given in Table 1. The locations of the elastic axis and of the center of gravity, respectively, are at 30 and 40% of the chord from the leading edge. The structural damping is assumed to be zero. It is not necessary to specify the chord length c and the natural frequency ω_θ. The frequency ratio σ is specified as 0.6; that is, the natural plunging frequency is three-fifths of the natural pitching frequency.

Table 1 Plate structural data

Property	Value
μ	20
σ	0.6
r	0.5
a	−0.4
x_0	0.2

Using the parameters given in Table 1, we solved Eqs. (8–11) numerically for a plate located very far from the ground. The motion was started with arbitrary initial conditions (disturbances). Here, we used $h_0 = 0$, $\dot{h}_0 = 0$, $\theta_0 = 0.05$, and $\dot{\theta}_0 = 0$. We increased the reduced airspeed gradually, starting very low and observing the behavior of the plate's responses.

Parts of the time histories are shown in Fig. 5 for two different reduced airspeeds: 2.02 and 2.10. Typical stable responses are shown in Fig. 5a. As the airspeed increases, the rate at which the responses decay decreases, and eventually, instead of decaying, a limit-cycle oscillation (LCO) develops, as shown in Fig. 5b. Thus, the numerical results predict that the aerodynamic damping is negative (causing decay) at airspeeds below, and positive above, a critical airspeed. Moreover, damping that is initially positive at small motions becomes neutral as the amplitude of the motion grows, a change that causes the growing motion to evolve into a limit cycle. The large initial disturbances cause large negative damping that rapidly drives the amplitude down to the limit cycle. The plate loses its dynamic stability when the airspeed is somewhere between 2.02 and 2.10.

The long-time histories for the reduced airspeed of 2.10 are plotted in Fig. 6, in which the development of an LCO is shown. The histories of the loads follow those of the motion closely. To determine whether the nonlinear aerodynamic model alone can be responsible for LCOs, we set $\cos\theta$ and $\sin\theta$ equal to 1 and 0. LCOs evolved for all numerical computations for airspeeds above critical. Including $\cos\theta$ and $\sin\theta$ in the aeroelastic model made the responses reach LCOs faster. This trend was also observed when cubic terms were included in the models of the springs.

To verify that limit cycles do develop, we solved Eqs. (8–11), starting the motion from four different initial conditions at a reduced airspeed of 2.1, which is greater than the critical airspeed. The initial conditions are $h_0 = 0$, $\dot{h}_0 = 0$, and $\dot{\theta}_0 = 0$, whereas θ_0 takes four values: 0.05, 0.15, 0.225, and 0.25. The phase planes of the pitching motion are shown in Fig. 7 for all four. The long-time responses are independent of these initial conditions, and all of the responses, some growing and others decreasing, reached the same limit cycle. The limit cycle is reached most quickly for the largest initial condition.

The amplitude of the LCO is plotted as a function of airspeed in Fig. 8. The higher the airspeed, the bigger the amplitude of the motion. The instability is a supercritical Hopf bifurcation. In designing airframes, subcritical instabilities are to be avoided, since they can lead to sudden large, often disastrous, responses.

Finding the critical reduced airspeed by increasing the airspeed gradually starting from a low value, as shown in Fig. 8, is time-consuming. We can apply a practical procedure based on the amplitudes of arbitrary limit cycles to find the critical airspeed.

For the supercritical Hopf instability, the following equation can be used for computing the critical airspeed V_c (Nayfeh and Balachandran [13]):

$$V_c = \frac{a_{\theta_2}^2 V_1 - a_{\theta_1}^2 V_2}{a_{\theta_2}^2 - a_{\theta_1}^2} \tag{12}$$

where V_1 and V_2 are above critical; a_{θ_1} and a_{θ_2} are the corresponding pitch amplitudes of the two LCOs (the reduced airspeed can also be

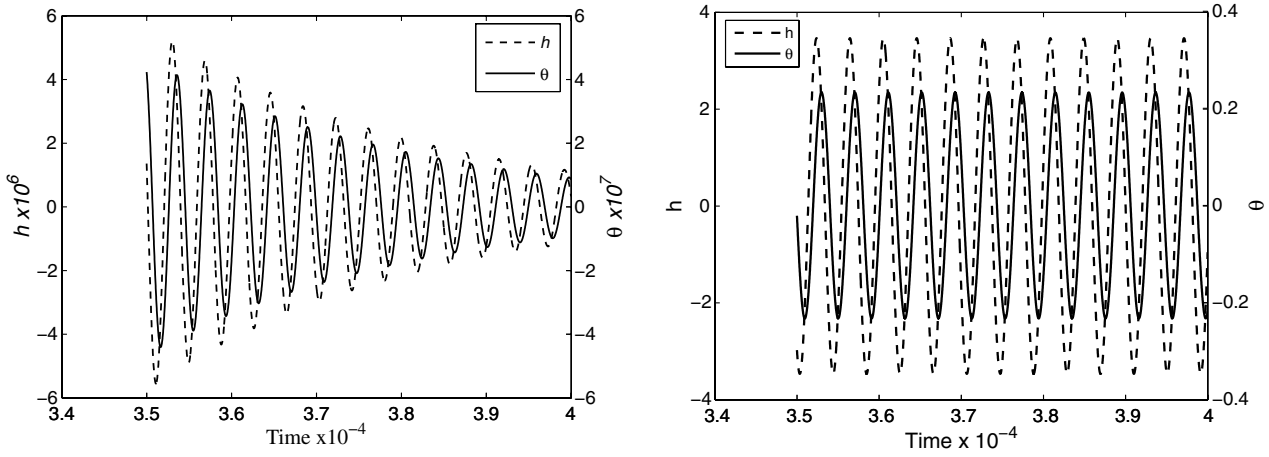

Fig. 5 Histories of the responses for two different reduced airspeeds a) $V = 2.02$ and b) $V = 2.10$, with the same initial conditions ($h_0 = 0$, $\dot{h}_0 = 0$, $\theta_0 = 0.05$, and $\dot{\theta}_0 = 0$).

found by using the plunging amplitudes a_h). Using two different reduced airspeeds, 2.10 and 2.11, both higher than the critical one, we calculated the response of a plate located far from the ground, found the two amplitudes of the motion, and inserted them into in Eq. (12). Part of the time history of their responses is shown in Fig. 9. The pitching amplitudes are 0.233 and 0.268; the critical reduced airspeed was found to be 2.07.

With Theodorsen's method, the value of the critical airspeed is obtained by first finding the flutter-frequency ratio ω_θ/ω_f that makes the determinant of Eqs. (5) and (6) zero by trial and error. For each value of $k = (c/2)(\omega_f/V_c)$, the coefficients l_h, l_θ, and m_θ are evaluated. Dynamic instability (flutter) occurs at the reduced frequency $k = 0.388$, and the flutter-frequency ratio ω_θ/ω_f is 1.23. Then V_c is computed by taking the reciprocal of the product of the reduced flutter frequency k and the flutter-frequency ratio ω_θ/ω_f is found to be 2.09. The agreement is good.

Theodorsen's method is limited to linear analysis, whereas the present method is not. Arbitrary angles of attack can be used with the present technique, whereas Theodorsen's method is limited to zero angle of attack. Moreover, Theodorsen's method can only provide the critical airspeed. It does not provide the transient motion leading to and developing after the static equilibrium position becomes unstable. It cannot predict a limit cycle or the characteristic of the instability, whether sub- or supercritical.

To promote more confidence in the present aeroelastic model and to provide some interesting results, we varied the location of the center of mass and calculated the critical airspeed. Again, the results are compared with those computed using Theodorsen's method, and again the agreement is good. The discussion is in the next section.

B. Effect of Ground

To expose the effect of the ground on the dynamic stability, we solved Eqs. (8–11) for the plate with the properties given in Table 1, moving near the ground at various dimensionless heights above the ground H and starting the motion with $\theta_0 = 0.05$. The remaining initial conditions $\dot{\theta}_0$, h_0, and $\dot{h}_0$ were set equal to zero. H is defined as the initial height of the elastic axis above the ground divided by the chord. Following the same procedure used to find the critical reduced airspeed out of ground effect, we found the critical speed to be 1.89 when $H = 0.50$. Part of the history of the response at H of 0.5 is shown in Fig. 10 for airspeeds of 1.94 and 1.95. The responses reached two different limit cycles. It should be mentioned that these airspeeds are below critical (2.07) for the same plate when it is out of ground effect. However, a common characteristic is that the peak in θ lags that in h. The ground has the effect of destabilizing the dynamic responses of the plate at lower reduced airspeeds.

The critical speed and the amplitude of pitching for an airspeed of 2.1 are plotted as functions of height above the ground in Fig. 11. The amplitudes of the limit cycles of the pitch angles increase as the height above the ground is decreased. The presence of the ground as well as the altered wake increase the effective angle of attack and make the magnitude of the aerodynamic loads larger in ground effect.

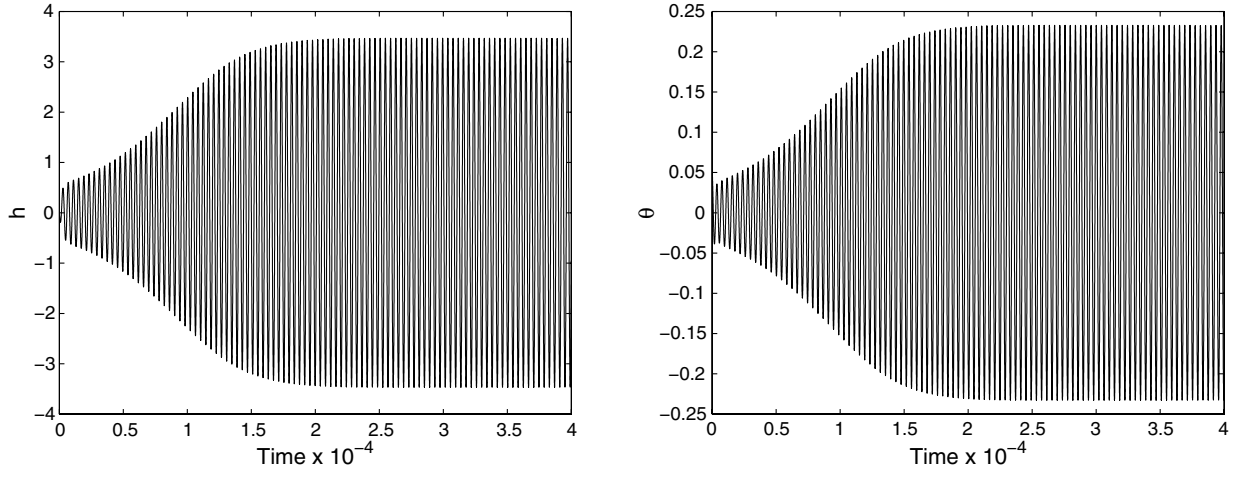

Fig. 6 Histories of the responses for reduced airspeed $V = 2.10$ that show the development of an LCO.

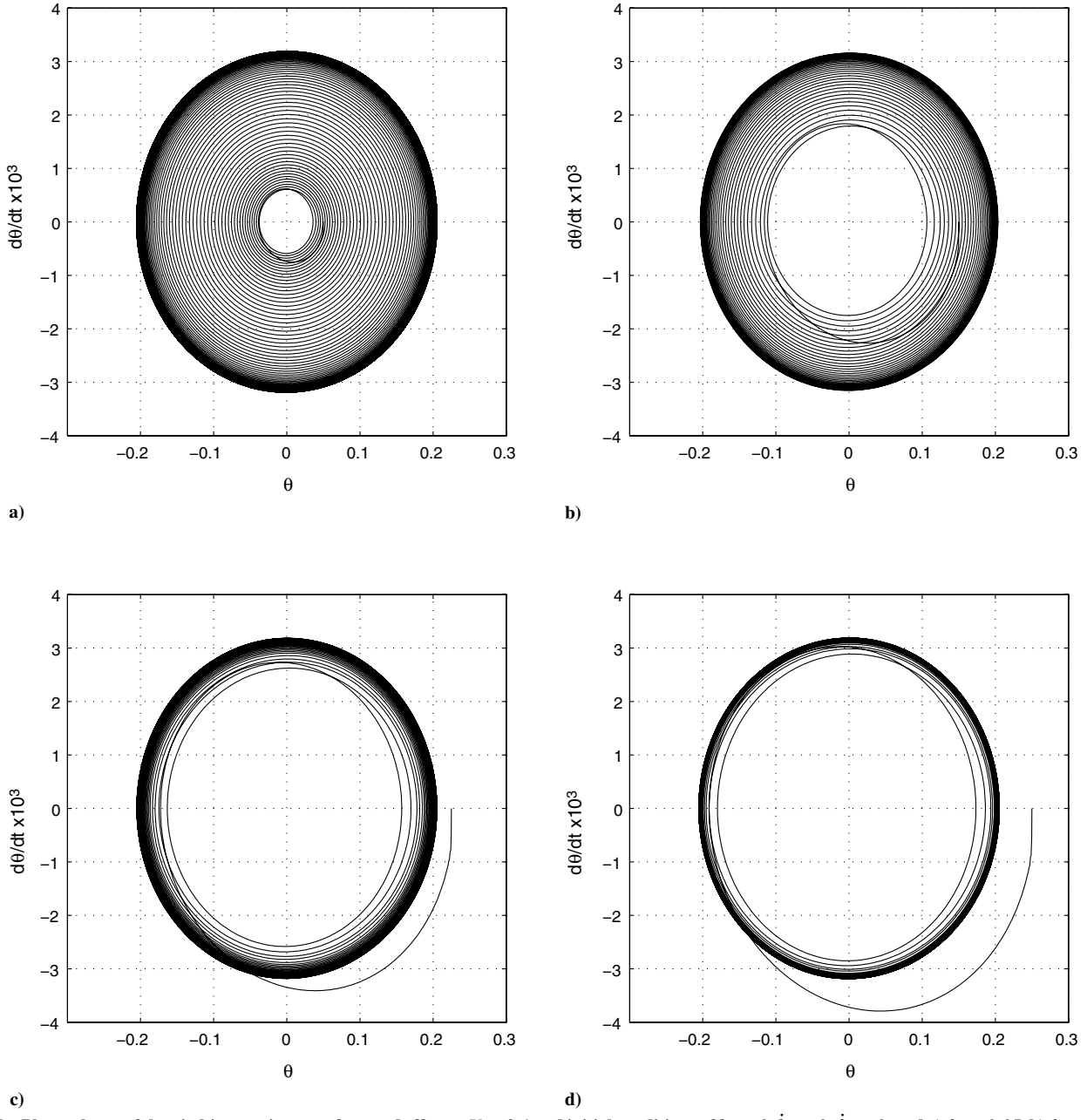

Fig. 7 Phase planes of the pitching motion out of ground effect at $V = 2.1$ and initial conditions of $h_0 = 0, \dot{h}_0 = 0, \dot{\theta}_0 = 0$, and a) $\theta_0 = 0.05$, b) $\theta_0 = 0.15$, c) $\theta_0 = 0.225$, and d) $\theta_0 = 0.25$.

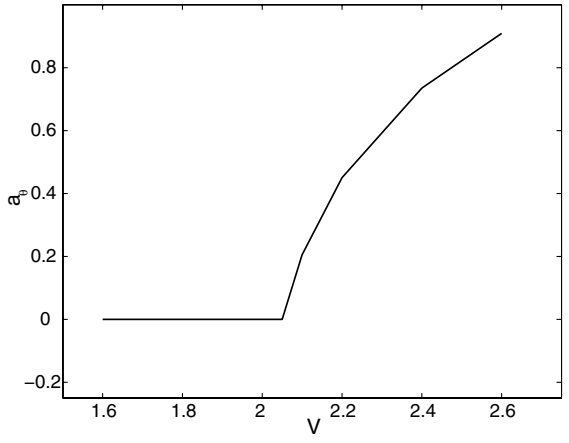

Fig. 8 Pitching amplitude vs reduced airspeed for a plate out of ground effect.

The effect of moving the center of mass, while the location of the elastic axis is fixed, is determined for plates far from and near to the ground. The present numerical results and those computed using Theodorsen's method are shown in Fig. 12. The agreement is good for the plates moving far from the ground. Moreover, as the location of the center of mass is moved, whether forward or backward, from the location given in Table 1 (i.e., $x_0 = 0.20$), the airspeed at which the plate loses its dynamic stability increases. The minimum critical airspeeds are shown to occur when the center of mass is aft of the elastic axis at a distance of $x_0 = 0.20$ for plates moving in and out of ground effect. The plate loses its dynamic stability at lower airspeeds near the ground.

C. Work Done for One Cycle

The work done for one cycle is computed for two cases. The first case is for a plate moving near the ground and the other is for the same plate executing the same motion far from the ground. The reduced airspeed is 1.95 so that the plate near the ground develops an LCO in response to an initial disturbance, whereas the response of the plate far

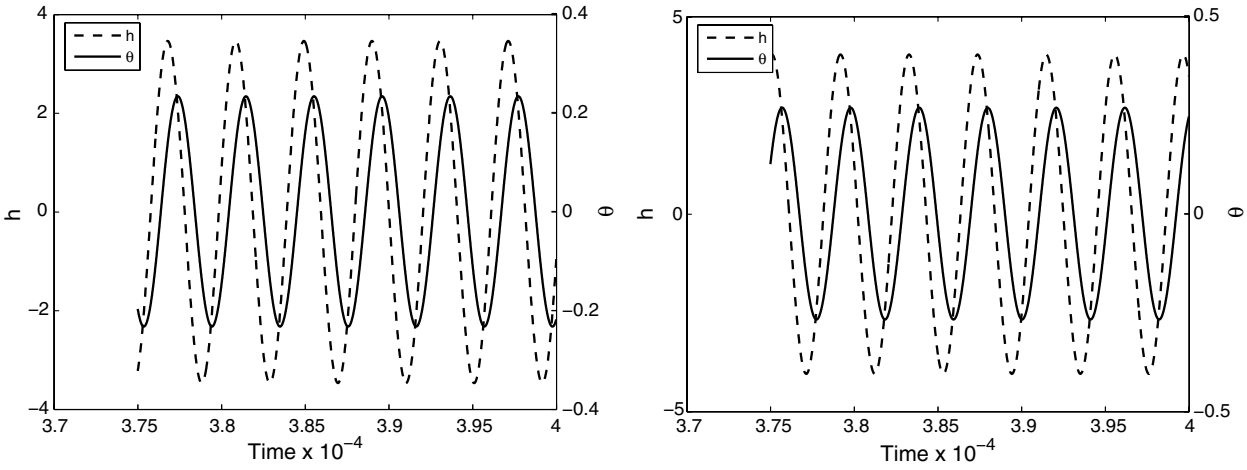

Fig. 9 Histories of the plate responses out of ground effect for two reduced airspeeds: a) $V = 2.10$ and b) $V = 2.11$ with same initial conditions used in Eqs. (12).

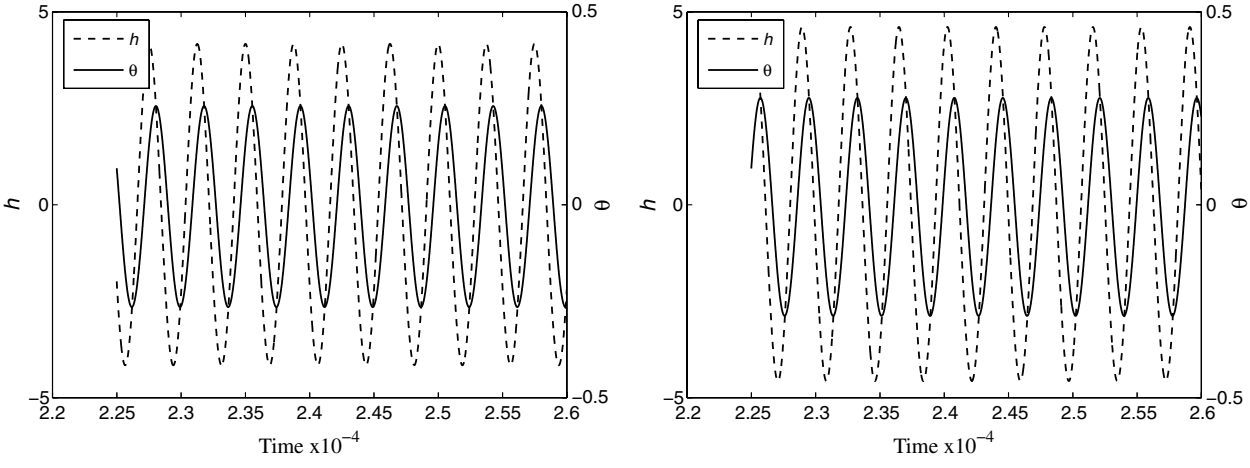

Fig. 10 History of plate responses at two different reduced airspeeds: a) $V = 1.94$ and b) $V = 1.95$ with the same initial conditions used in Eqs. (12).

from the ground decays to zero if the motion is not forced. Now the plate far from the ground is forced to have the same motion of the plate near the ground. The motions are the same, but the aerodynamic loads are different. Part of the histories of the aerodynamic loads for both cases is shown in Fig. 13. The magnitudes of both the normal-force coefficient C_n and the pitching-moment coefficient C_m are bigger for the case near the ground than they are for the case far from the ground. Moreover, the ground effect destroyed the symmetry of the normal forces by increasing the positive part; thus, in ground effect, the average C_n tends to lift the plate.

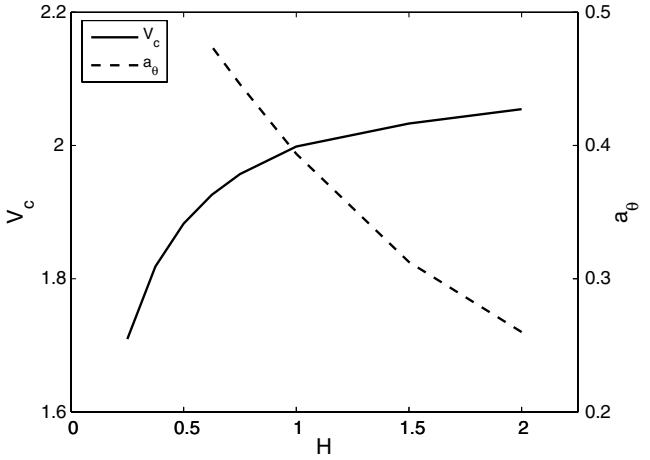

Fig. 11 Critical airspeed and pitch amplitude (for $V = 2.1$) vs the initial height of the elastic axis above the ground divided by the chord (H).

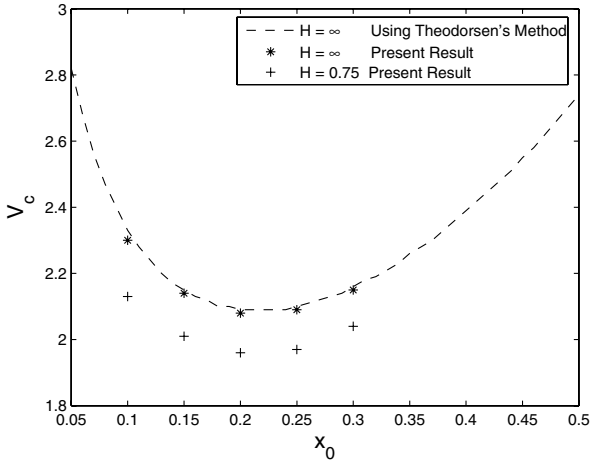

Fig. 12 Critical airspeed vs locations of the center of mass.

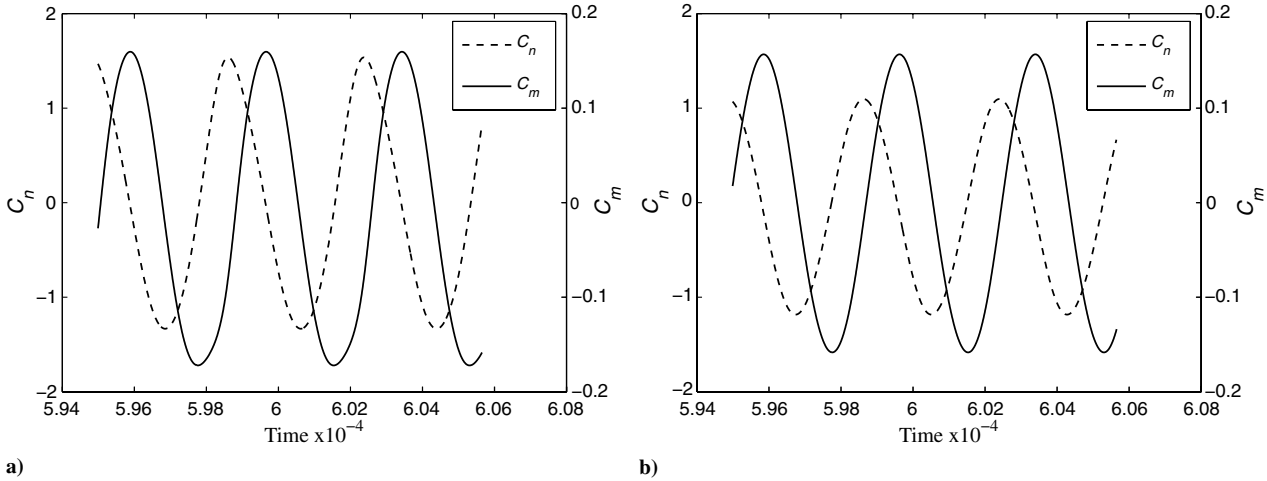

Fig. 13 Histories of aerodynamic loads: a) near the ground and b) far from the ground.

In addition, the lift and pitching moment coefficients are plotted as functions of positions in Fig. 14 for one cycle. The work done by the aerodynamic loads in both cases is computed for one cycle. As time increases, the point representing the lift moves in the clockwise direction, whereas that for the pitching moment moves in the counterclockwise direction, as shown in the figure by the arrows. The work done by the aerodynamic loads for the case near the ground is equal to zero, since the response is a limit cycle. For this plate, the work done by the lift force is 0.136, and that done by the moment is −0.136. For the plate moving far from the ground, the work done by the force is 0.078, that done by the moment is −0.119, and the net work done by the aerodynamic loads is −0.041; the positive work needed to overcome this aerodynamic damping is provided by the mechanism driving the plate. These results show that the negative work done by the aerodynamic moment is responsible for stabilizing the plate. The effect of the ground on the shape of the wake is partly responsible for changing the loads and destabilizing the plate, as discussed next.

D. Wake Shapes

A plate and its wakes (i.e., the locations of the vortices modeling the wake) moving near the ground at $H = 0.5$ are shown at the left

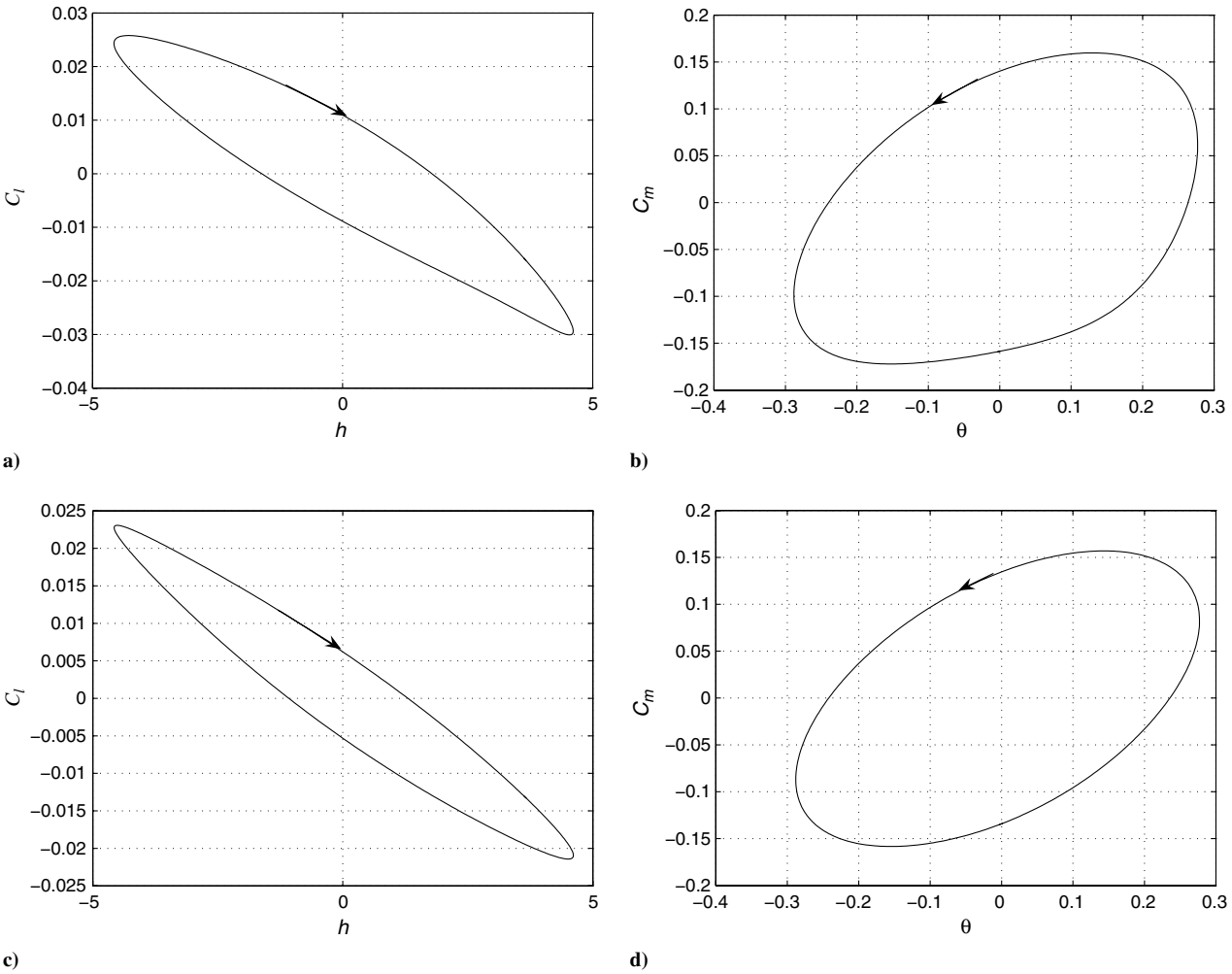

Fig. 14 Aerodynamic-load coefficients as functions of position for one cycle: a–b) near the ground and c–d) far from the ground.

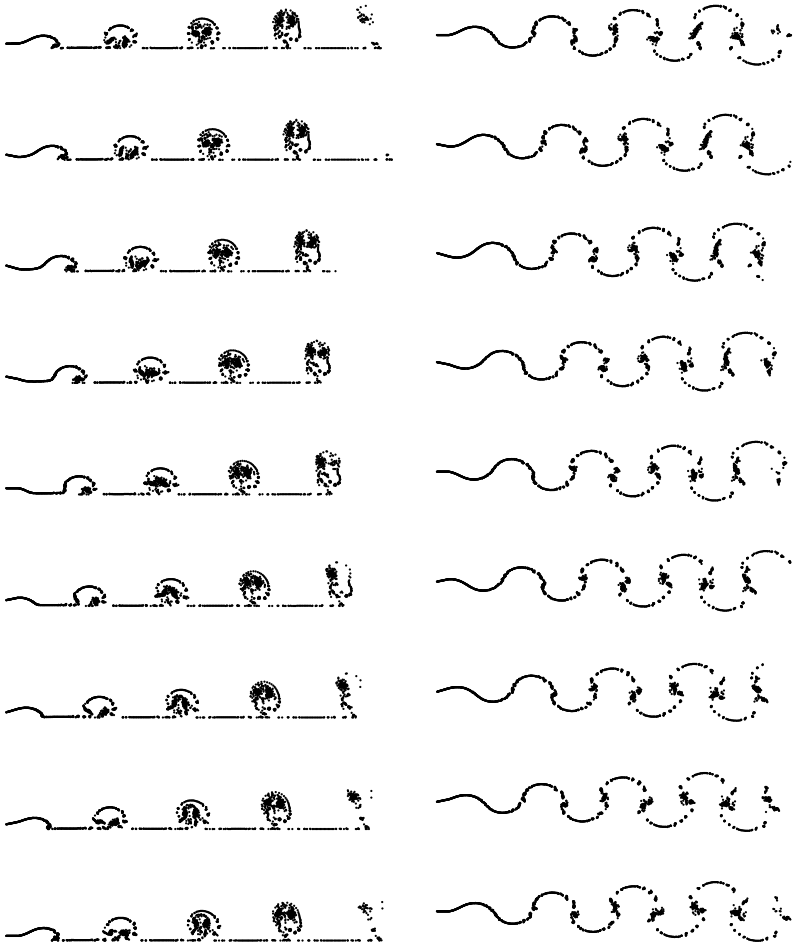

a) b)

Fig. 15 Wake shapes for LCOs: a) near the ground and b) far from the ground.

in Fig. 15 for one cycle after the motion reached an LCO. The plate position is shown with the thick lines at the left. The plots represent steady-state responses of the plate for the time interval starting at time step 60,188 and ending at 60,566. The plate and its wake are shown for every one-eighth of the cycle. The plate and its wake represented at the top correspond to the beginning of the cycle, and those at the bottom correspond to the end of the cycle. To show the effect of the ground on the wake shapes, the steady-state plunging and pitching responses for the plate moving near the ground at $H = 0.5$ and $V = 1.95$ are used as the prescribed plunging and pitching motion for the same plate moving far from the ground at the same airspeed. The aerodynamic model provides wake shapes and vorticity as part of the solution. The wakes of the plate moving far from the ground are also represented in Fig. 15. There are distinct differences. The ground destroyed the symmetry of wake shapes. The wake of the plate near the ground was prevented from moving downward when the plate leading edge moved upward, as seen with the wake of the plate far from the ground, and the

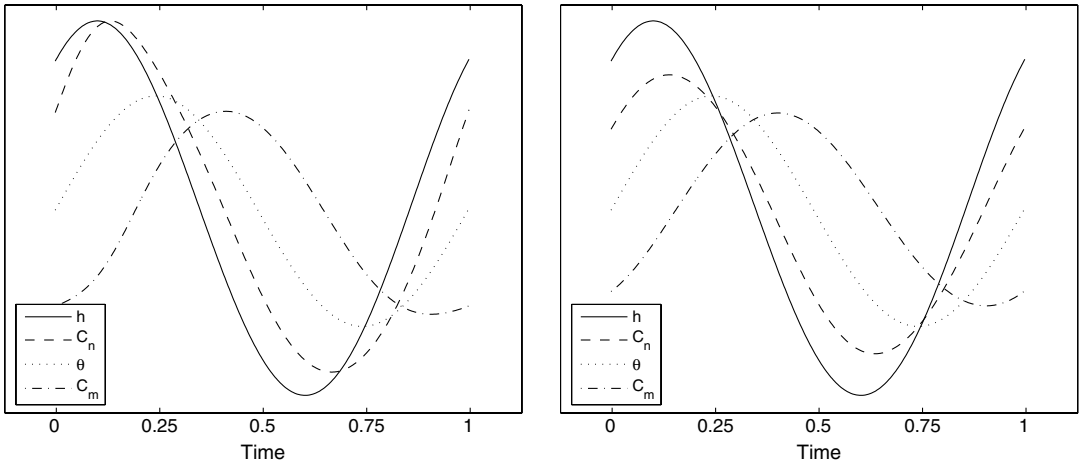

a) b)

Fig. 16 Plots of h, θ, C_n, and C_m for one cycle of the steady-state response: a) near the ground and b) far from the ground.

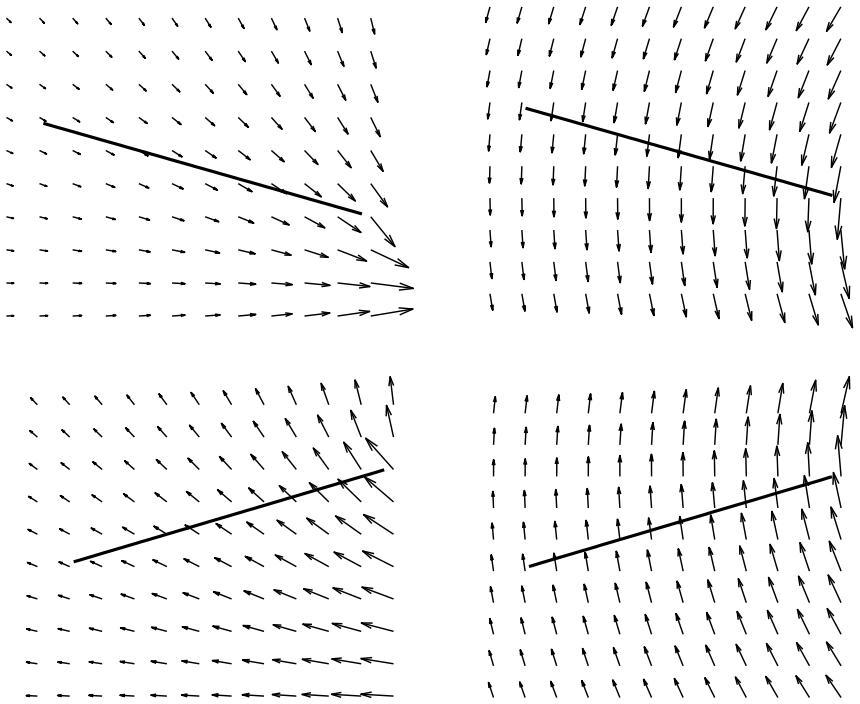

Fig. 17 Disturbance-velocity fields around the plate due to the vorticity of the wake at one-quarter of the cycle and three quarter of the cycle shown in Fig. 16: the plots at the left are near the ground and the others are far from the ground.

vorticity in the wake of the plate near the ground started to concentrate earlier.

The response and the loads for the cycle discussed above are given in Fig. 16. In both Figs. 16a and 16bθ, C_n, and C_m are magnified by factors of 10, 3, and 15 times, respectively. The loads lagged the motion. The magnitude of the normal force is bigger near the ground than far from it. Far from the ground, the loads were nearly symmetric, whereas near the ground, the normal force was affected by the ground and the symmetry of the loads disappeared so that the ground effect produced a nonzero average normal force.

In Fig. 17, the disturbance-velocity fields induced by the wake for these two cases are shown. The plots at the left are for the plate near the ground and the others are for the plate far from the ground. The top plots correspond to the end of one-quarter of a cycle, with the plate rotating clockwise at the instant depicted, and those at the bottom correspond to three-quarters of the cycles, with the plate rotating counterclockwise. The ground plane is a streamline for the plate near the ground. The magnitudes of the downwash on the plate are smaller for the plate near ground, which in turn increases the magnitudes of the pressure jumps and which increases the magnitude of the normal force. The magnitude of pitching moment is not affected very much. This may be the result of having the location of the elastic axis near the quarter-chord. Thus, the ground increases the effective angle of attack.

When the motion of the plate moving far from the ground at $V = 1.95$ is no longer forced, but computed using Eqs. (8–11), it decays to zero due to the fact that $V = 1.95$ is lower than the critical airspeed for the plate far from the ground, which is 2.07. To show the decay of the solution, the plate moving far from the ground with the prescribed motion of the plate moving near the ground is released and the plunging and pitching responses are computed using the aeroelastic model. The time histories of the plate's responses far from the ground after the release at time step 60,567 is shown in Fig. 18, and the wake shape is shown in Fig. 19. The motions of both the plate and the wake decay.

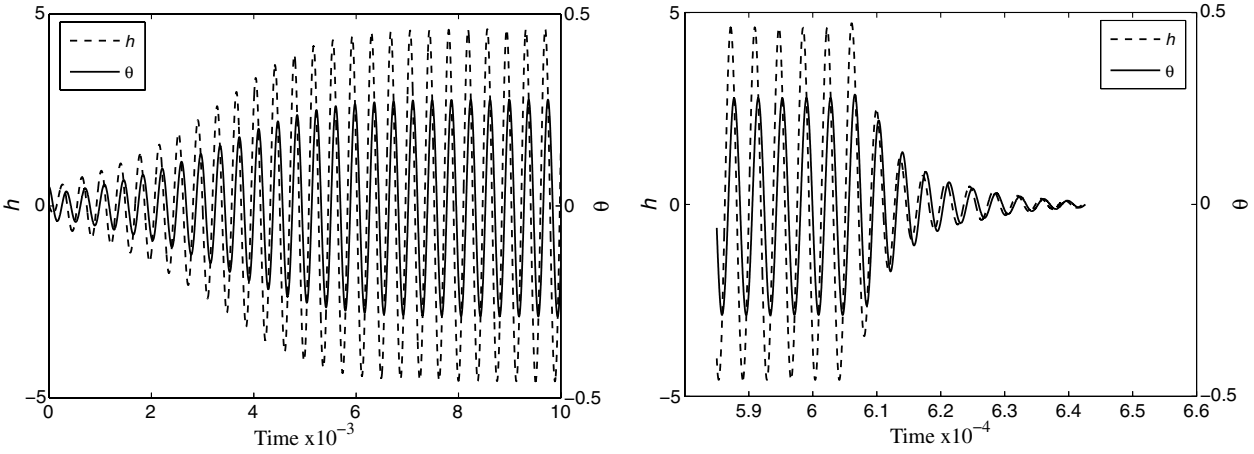

a) b)

Fig. 18 Histories of the plate's responses: a) in ground effect and b) far from the ground with the ground-effect motion imposed until the wing is released at an approximate time $\times 10^{-4} = 6.06$.

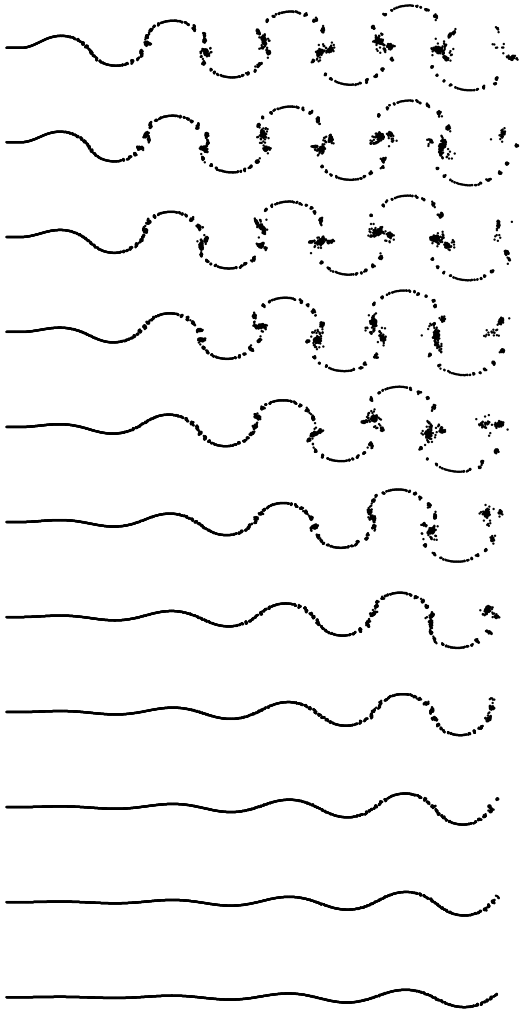

Fig. 19 Wake shapes far from the ground after release.

VI. Conclusions

An aeroelastic numerical model based on a 2-D unsteady vortex-lattice method has been developed and used to study the behavior of flat plates in a uniform flow near the ground. The ground effect is simulated by the method of images. The purpose of the present work is to disclose the effect of the ground on the dynamic stability of plates, and hence other effects such as flexibility, span, camber, thickness, twisting, and fluid viscosity are postponed to future investigations. Furthermore, no structural damping was included in the present model, since damping is expected to shift the onset of the flutter to a higher critical airspeed.

For plates away from the ground, some comparisons of the flutter speed obtained with the present simulation in the time domain were made with those obtained with Theodorsen's method in the frequency domain. The two sets of results were found to be in excellent agreement. The present simulation has some advantages over Theodorsen's method: it can model the transient motion before, during, and after the onset of flutter; it provides the nature of the flutter-causing instability, whether sub- or supercritical; it provides the disturbance associated with the wake and the effect of the ground on this disturbance, among others. The nature of the instability is important information, since subcritical bifurcations can lead to explosivelike motions. An understanding of the way the proximity of the ground affects aeroelastic behavior could be valuable for designers of very flexible UAVs intended for HALE missions. The present work is an initial step toward developing this understanding.

The proximity of the ground lowers the airspeed at the onset of flutter. The reduction in the critical airspeed is the result of the relatively sharp increase in the lift as the oscillating plate moves toward the ground and the decrease in the downwash the wake produces near the trailing edge. The latter strongly affects the lift and weakly affects the moment.

For low airspeeds, the plate does not flutter at all. For high airspeeds, the plate reaches limit cycles. The LCO is attributed to the nonlinearity of the aerodynamic model, since the structure is taken to be linear. LCOs evolved for all numerical computations at airspeeds above critical. Including $\cos\theta$ and $\sin\theta$ in the aeroelastic model made the responses reach LCOs faster. Moreover, including cubic nonlinear terms in the models of the springs also reduced the time for the motion to reach LCO. The present numerical study predicts the onset of flutter near ground at lower airspeeds than when far from the ground. Flat plates near the ground develop aeroelastic instabilities (flutter) similar to flat plates out of ground effect, but at lower airspeeds; the lower the height, the lower the critical airspeed. The proximity of the ground increases effective angles of attack and destabilizes the motion of plates. The results of the present study need to be validated experimentally.

Acknowledgment

The authors gratefully acknowledge the technical discussions with, and the suggestions of, Ali H. Nayfeh, especially in computing the onset of flutter.

References

[1] Theodorsen, T., "General Theory of Aerodynamic Instability and the Mechanism of Flutter," NACA Rept. 496, 1935.

[2] Theodorsen, T., and Garrick, I. E., "Mechanism of Flutter, a Theoretical and Experimental Investigation of the Flutter Problem," NACA Rept. 685, 1940.

[3] Scanlan, R. H., and Rosenbaum, R., *Introduction to the Study of Aircraft Vibration and Flutter*, Macmillan, New York, 1951; reprint Dover, New York, 1968.

[4] Fung, Y. C., *An Introduction to the Theory of Aeroelasticity*, Wiley, New York, 1955; reprint Dover, New York, 1993.

[5] Bisplinghoff, R. L., Ashley, H., and Halfman, R. L., *Aeroelasticity*, Addison-Wesley, Cambridge, MA, 1955; reprint Dover, New York, 1996.

[6] Bisplinghoff, R. L., and Ashley, H., *Principle of Aeroelasticity*, Wiley, New York, 1962; reprint Dover, New York, 2002.

[7] Hodges, D. H., and Pierce, G. A., *Introduction to Structural Dynamics and Aeroelasticity*, Cambridge Univ. Press, New York, 2002.

[8] Dowell, E. H., *Aeroelasticity of Plates and Shells*, Noordhoff International, Leyden, The Netherlands, 1975.

[9] Païdoussis, M. P., *Fluid-Structure Interactions, Slender Structures and Axial Flow*, Vol. 2, Academic Press, London, 2004.

[10] Nuhait, A. O., and Zedan, M. F., "Unsteady Ground Effects on Aerodynamic Coefficients of Thick Airfoils," *Arabian Journal for Science and Engineering*, Vol. 19, No. 4A, Oct. 1994, pp. 597–621.

[11] Nuhait, A. O., and Zedan, M. F., "Numerical Simulation of Unsteady Flow Induced by a Flat Plate Moving Near Ground," *Journal of Aircraft*, Vol. 30, No. 5, Sept.–Oct. 1993, pp. 611–617. doi:10.2514/3.46389

[12] Carnahan, B., Luther, H. A., and Wilkes, J. O., *Applied Numerical Methods*, Wiley, New York, 1969.

[13] Nayfeh, A., and Balachandran, B., *Applied Nonlinear Dynamics: Analytical, Computational, and Experimental Methods*, Wiley Interscience, New York, 1995.